Electro-Kinetics: A Viable Micro-Fluidic Platform for Miniature Diagnostic Kits

Hsueh-Chia Chang

Center for Micro-Fluidics and Medical Diagnostics, Department of Chemical and Biomolecular Engineering, University of Notre Dame, IN, U.S. 46556

INTRODUCTION

This review summarizes the current status of micro-fabricated DC and AC electro-kinetic devices. These devices promise to offer a viable micro-fluidic platform for miniature medical, environmental and security diagnostic kits. Their advantages include portability, precision and reliability. Several outstanding micro-scale scientific and design issues must be resolved before the technology can produce a fully integrated kit. Promising new research directions are also discussed.

The last decade has seen significant industrial and academic interests in micro-fluidics. Academic activities have reached a feverish level. National labs in the U.S., Japan, France, South Korea, Germany, Taiwan, China, Spain, etc. have all assembled large research groups in micro-fluidics. Major industrial labs like NTT in Japan and Motorola in the U.S. have also invested heavily in micro-fluidics research. All told, more than 20 micro-fluidic start-ups have been formed all over the world.

Such frenzy for micro-fluidic technologies is mainly driven by the vision that the various micro-fluidic components can be integrated into functioning devices for a variety of applications. The main advantages of micro-fluidic devices were thought to be their ability to handle a large number of small samples and the higher sensitivity they offer. Of these components, electro-kinetic components held and still hold the most promise. These are micro-fluidic devices that employ AC or DC electric fields to pump and mix fluids and to concentrate and sort beads, blood cells, bacteria, viruses and other particles. The electrodes that sustain these electric fields are integrated into the device and are often embedded within the micro-channels and micro-reservoirs. The only contact the device has with the periphery is than electrical without any material transfer. The peripheral equipment would typically be a battery-sized power supply, micro-transformers and/or chips for storage, control or transmission. Even with the peripheral electronics, the entire device could ideally be hand-held. In contrast, a syringe pump itself cannot be hand held and fluid needs to be transferred to the device through leaky connectors that must be hand connected for each application. Electro-kinetic devices are also much cheaper to fabricate than MEMS micro-fluidic components with moving parts and they often offer better flow control. In fact, MEMS research, be it purely mechanical or micro-fluidic, has almost completely faded in the last five years, with the inertial actuator in automobile airbags the only product to show. Micro-fluidic flows driven by the centrifugal force of a spinning CD player is also quite limited in application compared to electro-kinetics.

Nevertheless, after five years of intense research in electro-kinetics and other micro-fluidic platforms, a commercially successful device based on advanced micro-fluidic technologies has yet to appear in the market. A recent article in Bioscience Technology (DePalma, 2005) attributed this slow progress to over-emphasis on drug development and other laboratory products. As these micro-fluidic products will be used in laboratories, one major advantage of electro-kinetic devices has not been fully exploited: portability.

It is this reviewer's opinion that electro-kinetic components are most profitably integrated into portable chip-scale biosensors and diagnostic kits for the medical and environmental markets. The detection targets are pathogens (bacteria and viruses) in the medical and environmental samples. On-chip separation and counting of debris and blood cells are also important tasks on these kits that can be performed by electro-kinetic components. Most importantly, the portability offered by the electro-kinetic technology allows point-of-care application at home, in the field and next to the patient. To maximize this market potential, the products should be turnkey automated devices for the general consumer markets. They should not require visual examination by trained technicians with a microscope. As such, the devices should contain automated biosensors based on fluorescent labelling, optical absorption, electrochemical reaction, enzyme

* *Author to whom correspondence may be addressed.*
E-mail address:

immuno-assays, Raman scattering, PCR amplifications or even chip-scale mass spectrometry for organisms. The micro-fluidic technology hence becomes the enabling technology to enhance the speed and sensitivity of the biosensors on a chip platform. Development of the above biosensor technologies has nearly matured and it is an opportune time that they are integrated with the micro-fluidic technologies based on electro-kinetics. One could even envision the integration of wireless technology to such portable devices to supply the database for web-based personalized medical care and distributed remote monitoring of water supply.

However, despite the various advantages a micro-fluidic platform based on electro-kinetics offers, various technological obstacles remain before viable products can be realized. In pathogen detection, performance of any diagnostic kit with micro-fluidic technologies can be measured by the following metrics: specificity, robustness, sensitivity, portability and throughput. The first two criteria are sensor dependent and usually cannot be remedied by micro-fluidic technologies. The latter three, however, are very much sensitive to the micro-fluidic platform and will be scrutinized in this review for electro-kinetic devices.

We can reasonably expect a processing time of about 15 min with a hand-held micro-fluidic kit that can process no more than 100 micro-litres of sample solution. Longer and larger devices or smaller sample volumes would render the kit not portable, unattractive to the general consumer market and inferior to current diagnostic devices in terms of speed. If this sample needs to be transported across the chip through a micro-channel with a typical cross-section dimensions of 500x500 microns within the allotted 15 min (the total channel volume cannot exceed the sample volume), the necessary linear speed would be in excess of 1 mm/s, a linear flow velocity that still cannot be provided by electro-kinetic pumps with the highest throughput. Mechanical syringe pumps can exceed this high throughput of 100 nano-litres per second but they are usually large and not portable. Electro-kinetic pumps, at least the classical ones, are small and integrable into the small device but they often cannot produce a linear velocity that exceeds 100 microns/s and provide more than 10 nano-litres per second throughput. For the classical DC electro-osmotic pump (Zeng et al., 2001), one can employ an electric field no more than 100 V/cm as DC voltages in excess of one volt can easily produce bubbles in most samples. As the Zeta potential of all substrates do not exceed 100 mV, this translates into less than 100 microns per second of linear velocity, one to two orders of magnitude lower than the desired throughput. As such, electro-kinetic pumps must break the 1 mm/s barrier before it can provide sufficient throughput for realistic devices.

Sensitivity (or response speed) can be enhanced by micro-fluidic components in several ways. If liquid reagents, such as enzyme reagents in some immunoassays, need to be mixed, a micro-mixer can dramatically reduce the reaction time if the reaction is transport-limited. If a localized sensor is to detect a small number of pathogens on the chip, concentrating the pathogens towards the sensor can increase the diagnostic sensitivity. If the sample comes with blood cells, non-pathogenic bacteria and even debris, micro-fluidic components can separate or filter some of the bioparticles to allow the sensor better access to the target pathogens. We discuss some of these sensitivity issues below.

Pathogen detection for environmental and medical samples presents different micro-fluidic challenges. The number of target pathogen in an environmental sample is typically small and is often dispersed among other bacteria and viruses. For example, the number of hepatitis A virus, a common water pathogen in the third world, can be as small as 100 in one litre of water sample (Hedberg and Osterholm, 1993). Hence, a typical sample volume of 100 micro-litres for a micro-fluidic kit may not contain any pathogen and considerable filtration, incubation or PCR amplification is necessary before the pathogen count reaches detectable limits in micro-fluidic devices. In essence, a multi-litre sample needs to be reduced into less than one cc, with minimum pathogen loss, before micro-fluidic devices can be employed. The latter devices may be portable but the sample volume necessitates larger equipment. Integration with larger devices is hence a necessity when it comes to environmental monitoring. Virus and bacteria traps using charged membranes (nitrocellulose of Millipore HA, fibreglass and cellulose) and beads are being developed to concentrate environmental samples. They promise to replace the cumbersome centrifugal separation method that is not portable. However, release of pathogens by a small-volume eluting solution remains an imprecise technology. A technology that allows pathogen concentration without trapping within a membrane or a bead pack would be extremely desirable. This is a current research focus in our group but the issues will not be reviewed here. Even after filtration and concentration, there are typically less than 100 pathogens in a 100 micro-litre sample that must be detected and identified by a localized electrode. At this concentration, the average diffusion length towards the sensor is 1 mm and the diffusion time for the closest pathogen is nearly an hour, far exceeding the benchmark of 15 min. If all the pathogens need to be collected for quantification purposes, the collection time would be even longer. Sensitivity, as measured in response time, is hence a major micro-fluidic challenge even with the best sensors with fast kinetics. Electro-kinetic devices must reduce the transport time to the sensor to enhance the sensitivity.

Medical samples, on the other hand, have higher pathogen counts. For example, almost all the bacteria in the saliva sample of a TB patient would be TB bacteria. The challenge there is to identify the specific strain for proper antibiotic application. Hence, specificity offered by advanced immunoassays would need to be employed. Here, a multi-task immunoassay would require essentially a lab-on-a-chip platform with multiple streams, batches and integrated distributed flow control. Diagnosis of sepsis or other blood infection diseases typically involve only one bacteria species per patient. However, these bacteria need to be separated by the blood cells. There are typically five species of bacteria and fungi that can cause sepsis and their identification require PCR or immuno-assays that may also require elaborate micro-fluidic designs if they are to be performed on the chip.

In this review, we will examine how electro-kinetic technologies can meet the high throughput and concentration performance specifications and what new electro-kinetic devices and fundamental understanding of the underlying physics should be developed in the future. Portability advantages offered by electro-kinetic components are quite evident and will not be addressed further. The review will focus on engineering issues pertinent to diagnostic kit design. The readers are referred to a comprehensive review by Squires and Quake (2005) on the elegant multi-scale and match asymptotic mathematics and the careful experimentation that must be employed to describe and explore electro-kinetic phenomena.

DC ELECTRO-OSMOSIS (DC EO)

The most common electro-kinetic pump is a DC electro-osmotic (DC EO) pump (Zeng et al., 2001). Electro-osmosis depends on surface charges at the electrode/electrolyte interface. These surface charges result from the surface functional group and their interaction with the liquid medium. By integrating the Poisson equation across the surface charge and assuming negligible field on the solid side, the local field on the liquid side due to the surface charge E_s can be estimated to be σ_s/ε where ε is the liquid permittivity and σ_s the surface charge density. When coming into contact with a fluid that contains ions (either an electrolyte or a dielectric liquid with ionic impurities or generated locally via reactions). The surface charges attract counter-ions from the solution and repel co-ions from the surface to maintain local charge neutrality. Consequently, an excess of charges is built up near the electrode surface, thus forming an electrical double layer with thickness equal to the Debye screening length $\lambda = (\varepsilon RT/2z^2Fc_o)^{1/2}$, determined by a thermal Boltzmann distribution of counter-ions in the screened electric field generated by the surface charges. The permittivity ε, the Faraday constant F, the valency z for the symmetric ion pair and the ion concentration c_o all appear in the expression for the Debye layer. This double layer can be as thick as one micron for organic solvents and 10 nm for electrolytes with high conductivity $\sigma = 2F^2z^2c_o(D/RT)$. The counter ions screen the surface field such that it decays from E_s to zero rapidly over a distance of λ. The potential drop over this distance is the Zeta potential ζ.

The ions in the thin electrical double layer are mobile, and will migrate under the influence of an electric field tangential to the electrode surface. Due to fluid viscosity, fluid surrounding the ions will move along. Since there is an excess of counter ions, there is a net momentum transfer to the fluid resulting in a net flow called electro-osmosis. In a continuum description, a tangential Maxwell force is imparted on the fluid continuum within the charged double layer by the tangential field. The resulting velocity field has a high shear rate within the double layer but approaches a constant asymptote outside the thin layer. This slip velocity at the outer plane of the double layer is derived in the classical electro-kinetic literature (see, for example, Probstein, 1994)

$$u_t = -\frac{\varepsilon}{\mu}\zeta E_t \tag{1}$$

where E_t is tangential electric field, μ is the viscosity of the fluid, ζ is the Zeta potential drop across the double layer, which is an indication of charge density in the doubly layer. We note that DC EO velocity, unlike pressure-driven Poiseuille flow, is independent of the channel dimension. For weak polarization ($\zeta << RT/F = 24$ mV), the Zeta potential ζ can be estimated by $E_s\lambda$ and for larger polarization by $\zeta \sim 100$ mV (Israelchivili, 1992).

For most channel materials with moderate surface charged density in typical electrolytes, the Zeta potential is less than 100 mV and the DC electro-osmotic mobility is less than one (micron/s)/(V/cm) or 100 microns/s linear velocity per 100 V/cm field applied. This low mobility usually cannot meet the throughput performance of most units, as discussed earlier. Moreover, DC voltages in excess of 2 V will produce bubbles even with dielectric coating and hence their electrodes must be housed in open reservoirs at the ends of the micro-channels to allow release of the bubbles. As most channels are at most a few cm long, a minimum velocity of 1 mm/s can only be produced by over 100 volts of DC field. Such a high DC voltage is dangerous for biological fluids with high conductivity.

If, however, high throughput (linear velocity) is not required, DC EO pump can be used to produce high pressure necessary to pump fluids through sub-micron channels or channels with porous chromatograph packing. The pump pressure can be maximized by packing the channel with a high surface charge medium or beads. The pump pressure is generated by flow balance. If the tangential electric field E_t is applied along an entire channel with uniform surface charge, the velocity profile would be flat at every position and equal to u_t. However, if the electric field is applied only over the pump section and not over the load section, there would be no electro-osmotic flow in the latter section. However, flow balance dictates that the flow must be the same in both sections of the same channel. This can only be true if a piece-wise linear pressure distribution is established along the channel with the maximum at the junction of the two sections. The constant pressure gradient in each section is such that the flow rates are the same in both sections. In the load section, if it is a rectangular channel without side boundary effects, a pure pressure driven flow results with a Poiseuille flow profile of

$$u_l(y) = \frac{1}{\mu}\left(\frac{\partial p}{\partial x}\right)_l \frac{y}{2}(y-d) \tag{2}$$

In the pump channel, a frustrated flow results from a linear combination of the flat DC EO flow and a pressure driven Poiseuille back-flow,

$$u_p(y) = \frac{1}{\mu}\left(\frac{\partial p}{\partial x}\right)_p \frac{y}{2}(y-d) + u_t \tag{3}$$

Flow balance then stipulates that the two pressure gradients are related by

$$\left(\frac{\partial p}{\partial x}\right)_l = \left(\frac{\partial p}{\partial x}\right)_p - \frac{12\mu u_t}{d^2} \tag{4}$$

It is clear that the load pressure gradient increases in amplitude with larger electro-osmotic velocity in the pump section and with smaller channel dimension d or higher effective viscosity μ. This motivates the use of a high surface-charge density porous substrate in the pump section with a small pore radius (Wang et al., 2006). However, the above argument breaks down when the pore radius becomes smaller than the double layer thickness λ, as the slip velocity derivation was obtained for $d >> \lambda$. In fact, the maximum pressure gradient in the load section occurs when the pore radius is the same as the double layer thickness. When the pore size is smaller than the double layer thickness, the net charge begins to diminish as the entire pore becomes charged but with fewer counter ions. This reduction in net charge overcompensates for the pressure build-up of smaller pores to reduce the load pressure gradient.

Chen et al. (2005a, b) have used so-gel chemistry to synthesize nano-porous silica beads that fuse to generate a porous monolith with a pore size of about one micron. The synthesis is carried out in a silica capillary and the substrate is fused directly to the capillary wall as seen in Figure 1. This fusion of substrate and capillary housing creates a continuous porous monolith of high mechanical integrity (no channelling) and strength to sustain the high pressure without leakage. The pore dimension of one micron is also compatible with the thicker double layers of organic solvents. As seen in the pump curve of Figure 2, back pressure in excess of 1 atm can be generated in the 100 micron capillary with a silica monolith for many organic solvents. This high pressure is sufficient to pump the sample through

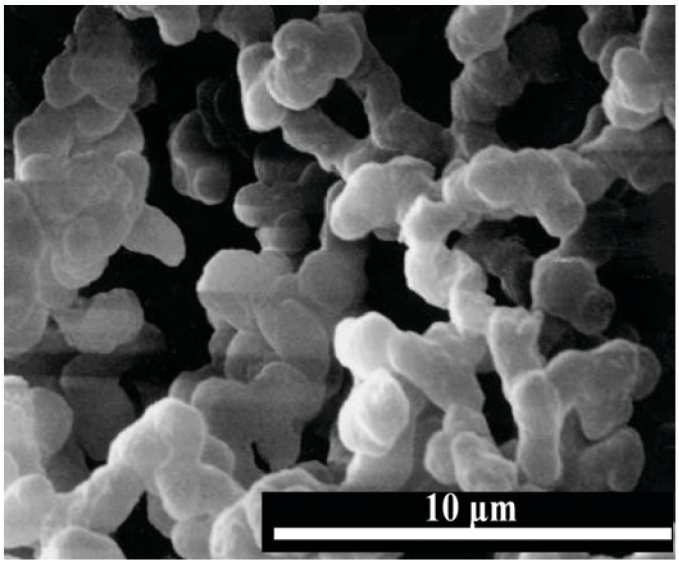

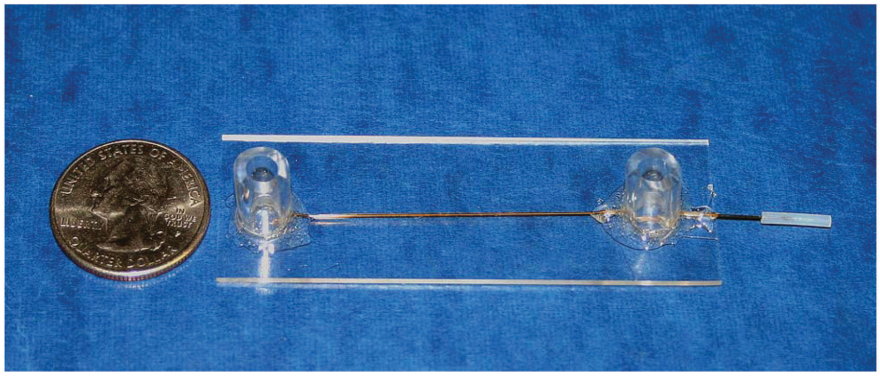

Figure 1. A silica monolith consisting of fused nano-porous silica beads are[is or that are?] synthesized within a 100-micron silica capillary by sol-gel chemistry. The silica beads also fuse with the capillary to form a substrate of high integrity. The DC EO pump with two external electrode reservoirs are shown in the bottom image. The electrodes are enclosed in a Nafion housing to prevent bubble invasion into the pumping channel. Electrosprays can also be emitted at the end of the capillary.

micro-chromatograph packing and through DC spray micro-needles for mass spectrometry (Chen et al., 2005b). However, the highest throughput is less than 50 nano-litres per second, which is high for DC EO pumps but is still inadequate for most rapid diagnostic kits.

FIELD INDUCED ELECTRO-OSMOSIS

There are two known DC (and AC) electro-kinetic phenomena whose charge polarization is not due to the surface charges on the surface. Instead, their surface charge is induced by the applied field and is hence independent of the surface chemistry. The field-induced polarization can be due to capacitive charging of bulk electrolyte ions into the double layer near the surface or by dielectric polarization of the surface substrate and medium molecules by the penetrating field. If such field polarization is possible, the effective Zeta potential is often much larger than the natural Zeta potential and hence gives rise to much larger throughput than DC EO. As these field-induced phenomena require the applied field to penetrate the surface, the applied field must overcome the screening effect by counter-ions in the double layer. For most material, the double layer field $E_s \sim \zeta/\lambda$ is of the order of 100 V/cm and hence field-induced polarization typically occurs for applied fields in excess of 1 kV/cm. Even with this large field, if the substrate has zero conductivity or permittivity, field penetration into the substrate or the double layer above it is weak at best.

There are, however, two exceptions that allow significant field penetration. One concerns a conducting ion-exchange granule that attracts the bulk field lines, the so-called nonlinear electro-kinetic phenomenon of the second kind (Dukhin, 1991; Ben and Chang, 2002). Here, due to field penetration across the conducting granule, the potential drop over the extended double layer due to field-induced polarization is of the order Ea, where E is the applied field and a the granule dimension. For larger granules of nearly 1 mm in dimension and with a field of 100 V/cm, this polarization can produce an effective potential of 10 V and a linear velocity exceeding 1 cm/s (Barany et al., 1998; Ben et al., 2004). In principle, the same super-polarization can also be achieved with a porous surface on a channel, which is a promising research direction.

Field-induced polarization can also occur on a substrate with a finite permittivity, provided the external field is in excess of $E_s \sim \zeta/\lambda$. This occurs at sharp substrate corners where the channel geometry produces a singular tangential field at zero substrate permittivity and a large tangential and normal field at finite substrate permittivity (Thamida and Chang, 2002). There the effective potential drop across the double layer due to field-induced polarization scales as $\kappa E\lambda$ multiplied to a geometric factor corresponding to some power of the ratio of the channel dimension to the radius of curvature of the corner, where κ is the ratio of wall permittivity to medium permittivity. Since the geometric factor is large for a sharp corner, this effective potential is typically much larger than ζ and the resulting electro-osmotic velocity is often in excess of 1 mm/s.

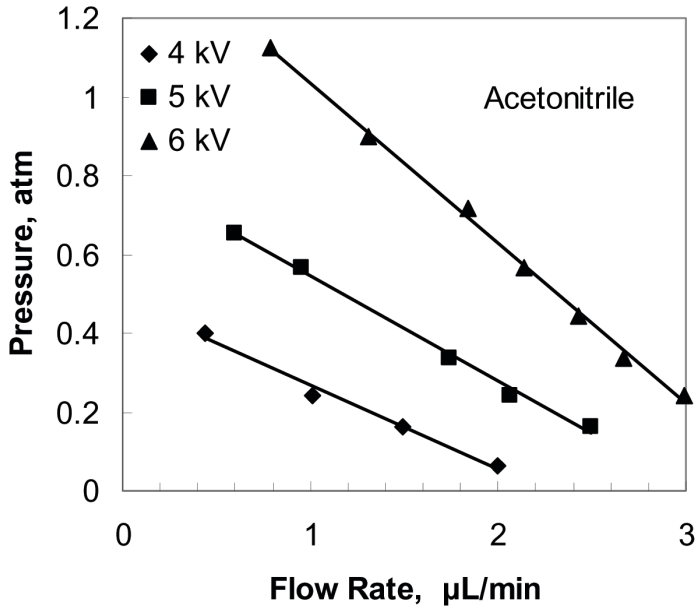

Figure 2. The pump curves for the DC EO pump of Figure 1 at different voltages and with acetonitrile as the pumping fluid. Organic solvents like methanol, ethanol and acetone have also been successfully tested. The throughput is less than 50 nano-litres per second but the pressure can reach 1 atm in a 100 micron capillary.

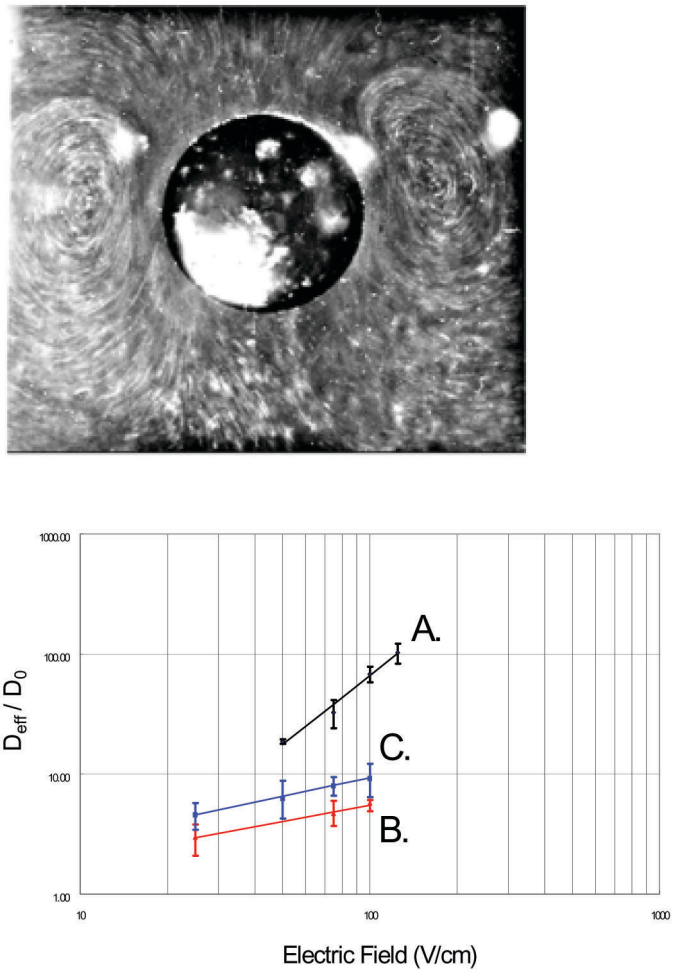

Figure 3. Vortices generated by field-induced polarization at a conducting granule. The effective diffusivity of a drop of dye placed near the granule is determined by the temporal variations in the grey scale of the pixels from a video movie. Curve A is with the granule and B and C are mixing due to DC EO flow without the granule and the mixing vortices. The estimated diffusivity is normalized by true molecular diffusivity of the dye. The effective mixing is seen to be enhanced by a factor of 100 due to the vortices.

In all the above examples of field-induced polarization, the normal field and the polarization are not uniform if only a single set of electrodes is used. Consequently, vortices driven by pressure-driven back flow, like that in DC EO flow of non-uniform polarization, often appear. These vortices can achieve very rapid mixing for transport-limiting reactions (Wang et al., 2004; Takhistov et al., 2003). In Figure 3, the vortices around a conducting granule are seen to mix a food dye with a mixing time two orders of magnitude lower than pure diffusion.

However, if pumping action is desired from field-induced DC EO flow, special substrate geometries must hence be designed to eliminate vortex formation and affect a net flow. Unfortunately, it is difficult to coat channels of unusual geometry with a conducting porous membrane (or to design them with a continuum of corners) to produce a sustained electro-kinetic flow. Coating with surfactants, dielectric films of high permittivity or fractal material with large conductivity are promising future research directions for this phenomenon. These future devices however, would most likely utilize multiple electrodes: a set for polarizing the surface with uniform polarization and another orthogonal set for providing the tangential field E_t to drive the flow.

AC ELECTRO-OSMOSIS (AC EO)

A more practical means of circumventing the low throughput limit of DC EO is by AC EO (Gonzalez et al., 2000; Ajdari, 2000) shown schematically in Figure 4, which suppresses undesirable reactions by energizing the electrodes with high-frequency electric fields (> 1 kHz) whose period is shorter than the charge transfer (electro-chemical reaction) time at the electrode. Similar to DC EO, AC EO is also generated by exerting a force on double layer charges at solid/liquid surface by tangential electric fields. However, the relevant charges in AC EO flow are no longer the permanent surface charge of the channel but the induced charge from the bulk electrolyte to the electrode surface. The electrical potentials over electrodes induce net charges in the electrical double layer and in the meanwhile provide tangential electric fields to drive the ions. Because charges in the double layer and electric fields change directions simultaneously, AC EO produces steady local vortices above two disjoint electrodes, as shown in the actual computed flow fields of Figure 5.

Based on the work by Gonzalez et al. (2000), the charging of the electrode double layer by the bulk field can be approximated by a distributed set of differential RC elements,

$$\sigma \frac{\partial \phi}{\partial y} = C_{DL} \frac{\partial}{\partial t}(\phi - V_o) \tag{5}$$

where the left hand side is the local current per unit area from the bulk and the right is the charge accumulation at the electrode measured in terms of the potential difference between the value of the bulk potential ϕ at the electrode and the AC voltage $V_0(t)$ at the electrode. (The original equation by Gonzalez et al. (2000) is in the frequency domain after a Fourier transform in time.) The capacitance per unit area of the electrode double layer is $C_{DL} \sim \varepsilon/\lambda$. The electric field in the bulk can now be solved from the Laplace equation with Equation (5) as a boundary condition.

The time-averaged slip velocity on the electrode is then

$$u_{AC-EO} = -\frac{\varepsilon_m}{4\mu} \frac{\partial}{\partial x} |\phi - V_0|^2 \tag{6}$$

where the vertical bars stand for the amplitude of the time-periodic quantities within them. The equation represents the effective slip velocity on the electrode surface. If values of the electric field are known, the steady bulk fluid velocity can now be solved using the Stokes equation with Equation (6) as a boundary condition, the time periodicity of the electric field has been removed in this time-averaging formulation.

The key advantage of AC EO vs. DC EO is evident in Equation (6). Unlike the classical DC EO in Equation (1) with a linear scaling with respect to the field, the AC EO slip velocity scales as the square of the applied voltage (or field). If the electrode separation, i.e. the x length scale is identical for both AC and DC EO flow, comparing Equation (1) to (6) suggests that the effective Zeta potential for AC EO flow is the applied voltage V_0, which is typically much larger than the Zeta potential ζ. In actual fact, the enhancement in mobility is even greater. The applied voltage V_0 for AC EO can be much larger than that in a DC EO as the high frequency eliminates electrode reactions like electrolysis and bubble generation. In Figure 6, the bubble regime of AC EO flow at different frequencies and voltages are shown. It is evident that at 1 Mhz, the applied voltage can exceed 20 V without bubble generation, in contrast to the bubbling voltage of 1 V for DC electric fields. Moreover, the AC electrodes can be embedded directly in the channel and can be much closer than DC electrodes. These factors and the quadratic scaling with respect to field have generated AC EO velocities in

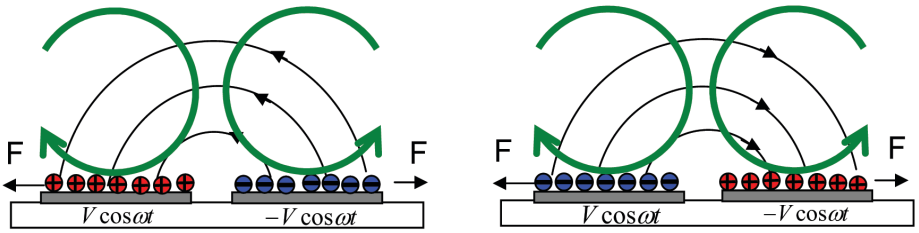

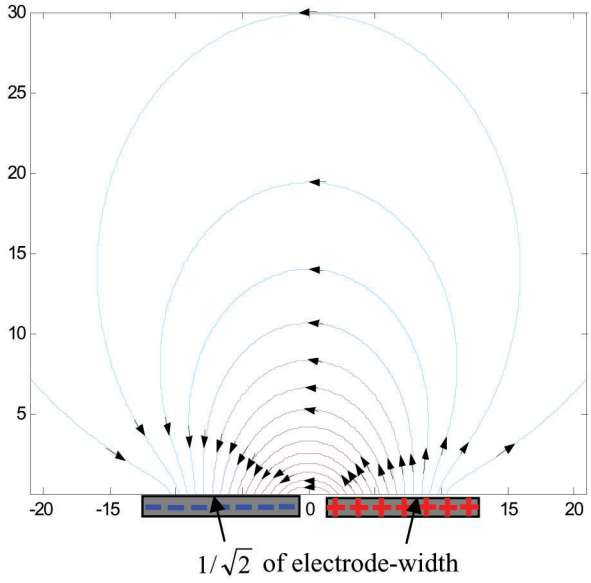

Figure 4. The top diagram depicts AC EO capacitive charging of two symmetric planar electrode surfaces over two half-cycles of the AC field. The Maxwell forces are indicated with back arrows. Although the field changes direction after each half cycle, so does the field-induced polarization due to capacitive charging. As a result, the net Maxwell force and the slip velocity is always outwards at the inner edges of the electrodes. The bottom diagram shows the field lines at low frequencies. The two electrodes behave line constant-flux line sources and the tangential field direction changes at $1/\sqrt{2}$ of the electrode width. The slip velocity becomes inward beyond that position which corresponds to a converging stagnation line.

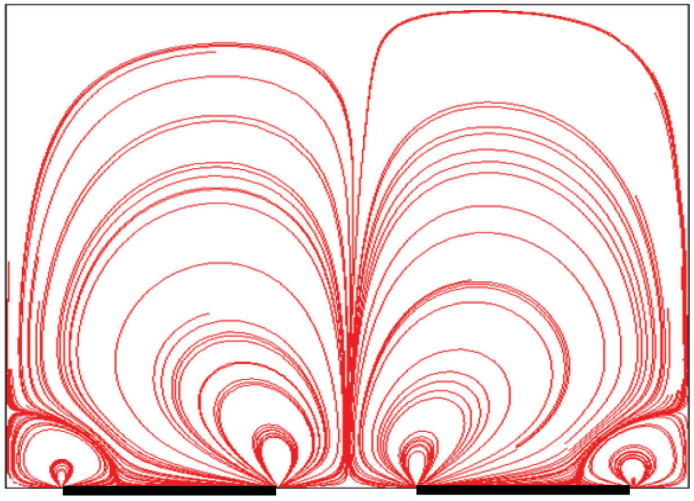

Figure 5. Simulated AC EO flow above two parallel electrodes indicated by dark lines. Other than the converging stagnation line at $1/\sqrt{2}$ of the width, there is a stagnation flow at the electrode gap and small vortices at the electrode ends due to singular Maxwell forces at the corners.

excess of 1 mm/s (Ramos et al., 2003), a major step towards electro-kinetic pumps with high throughput.

At low frequencies, the electric and flow fields of two disjoint parallel electrodes can be estimated (Ben and Chang, 2006). As the Laplace equation and the equivalent electrostatic condition Equation (5) are linear, a Fourier transform in time can be carried out. The only effect is the transformation $\frac{\partial}{\partial t} \rightarrow i\omega$ in Equation (5). A low frequency ω expansion can then be carried out. The leading order solution with an insulated boundary condition Equation (5) is a constant potential general solution that can be omitted. The boundary condition Equation (5) becomes one of constant flux for an imaginary potential and the problem becomes two constant-flux line sources with dipole-like field lines. A simple analysis for very wide electrodes (the electrode width is much larger than the electrode separation), shows that the tangential electric fields switch directions at $1/\sqrt{2}$ of electrode-width away from its inner edge, the golden ratio. Because flow directions depend on the tangential fields as seen in Equation (6), four counter-rotating vortices were formed at the electrode surface, and the stagnation takes place at locations where tangential fields become zero, as shown in Figure 4.

Even larger fields and voltages can be applied if one uses the wire geometry (Gagnon and Chang, 2005) shown in Figure 7

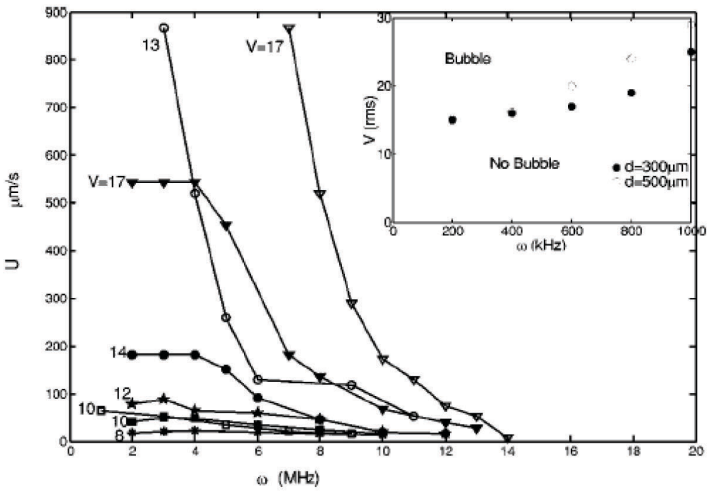

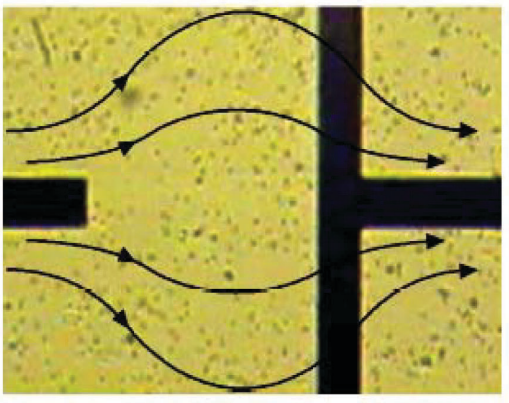

Figure 6. Planar T electrode arrays about 50 microns wide and the measured linear velocity as a function of voltage and frequency. The insert indicates the critical voltage for bubble generation is a function of frequency, reaching 20 V at 1 Mhz.

instead of the two disjoint electrodes in Figures 4 and 5. As the current prefers to traverse along the wire instead of through the bulk electrolyte, electrochemical reaction does not occur up to 100 V! The largest potential drop is across the last two segments of the wire as shown in the computed field lines and two large AC EO vortices with linear velocities in excess of 1 cm/s are observed. Higher voltages in excess of 1 KV can be sustained by using a dielectric coating on the wire and using a zwitter ion that increases the permittivity and coats the wire surface (Gagnon and Chang, 2005).

For both the disjoint electrode and the wire electrode, AC EO flow has a maximum with respect to the AC frequency ω. As seen in Equation (5), the double layer is fully charged at low frequency and the resulting screening removes any bulk field, $\frac{\partial \phi}{\partial y} = 0$, and any AC EO flow as seen in (6). However, at very high frequencies, there is no charging and the bulk field at the electrode is equal to the constant electrode potential $\phi = V_0$. In this case, the period is too short compared to the charging time and there is no surface polarization. The effective AC EO velocity also vanishes at this limit as seen in (6). Hence, the optimal frequency is the inverse charging time or RC time of the RC circuit, $\sigma/C_{DL}\lambda = D/\lambda L$ in (5), where the Debye screening length is taken to be the y length scale. Using a typical electrolyte with conductivity and permittivity ($\sigma = 100$ mS/cm, $\varepsilon_m = 80$), the measured fluid slip velocities of the wire geometry at different voltages are shown in Figure 7 to share a common optimum frequency of about 100 Khz, roughly equal to D/λL for the electrolyte used and the specific electrode separation.

As the symmetric disjoint and wire designs produce only vortices with no net flow, they represent good micro-mixers without the introduction of granules as in Figure 3. However, to achieve a net through flow without vortices, the AC EO pump must employ asymmetric electrodes. It is the selection of the proper asymmetric electrode geometry to achieve maximum AC EO pumping that is the most difficult part of designing this micro-pump. Designs like asymmetric parallel electrodes (Ramos et al., 2003) and T electrodes, see Figure 6 (Lastochkin et al., 2004) and converging coils (Gagnon and Chang, 2005) have been reported. The converging coils produce the largest throughput, as large as 100 micro-litres per second for low loads. Also, since only the electrode surface is polarized, the largest throughput is obtained with maximum electrode coverage. This is again an advantage of the coil design. Although a pump curve like that of Figure 2 has yet to be measured for AC EO pump to determine the highest pressure it can sustain, it is clear that the high-throughput barrier of DC EO pump has been overcome by properly designed AC EO pump. Moreover, there is evidence that, at larger voltages, Faradaic polarization due to electro-chemical reactions at the electrodes contribute significantly to AC EO flow. An optimal frequency at the inverse RC time is often missing and the scaling of the AC EO velocity with respect to the voltage is exponential rather than quadratic as predicted by Equation (6) Lastochkin et al. (2004). In fact, Faradaic polarization has been observed and shown to reverse the AC EO flow direction predicted by Equation (6) (Wu et al., 2005; Ben and Chang, 2006). Field-induced polarization on an electrode is hence far from being fully understood.

As for pumps based on DC field-induced polarization, another fruitful research direction for AC EO pumps is the use of multiple sets of synchronized electrodes or wires, with one set producing uniform polarization and another orthogonal set supplying the tangential field. The polarizing electrodes could be covered with a high permittivity dielectric coating or a conducting porous film to increase its capacitance. In fact, it is quite possible that AC field-induced polarization, like that for DC, can be achieved on dielectric film coated channel surfaces instead of only on the electrode surfaces. This AC EO pump based on field-induced polarization on substrates would greatly increase the pumping area and the throughput. It also eliminates the necessity to cover the channel with embedded asymmetric electrodes, which are difficult to design. Nevertheless, even in its current version, AC EO mixers and pumps can already meet most of the throughput requirements of diagnostic kits, which is a major breakthrough for electro-kinetic devices.

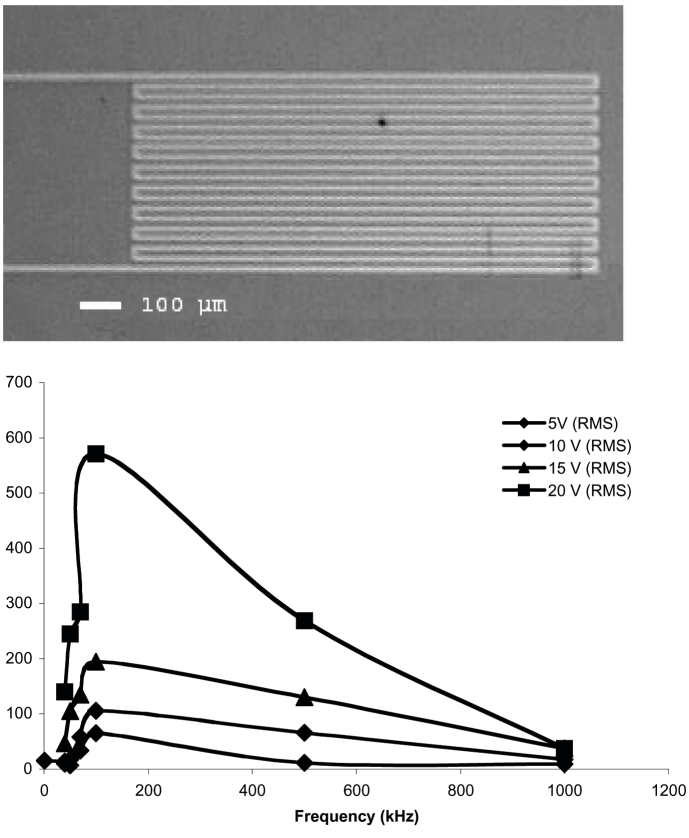

Figure 7. The wire AC EO pump with a continuous planar wire coated with a dielectric film. The measure slip velocity shows a maximum at an optimum frequency corresponding to D/λL.

AC DIELECTROPHORESIS (DEP)

The DC EO and AC EO flows involve Maxwell forces on the liquid to produce liquid convection. Particles within the liquid will also be convected at the liquid velocity, as particle inertia is typically negligible for particles within micro-fluidic devices. However, convective transport of particles cannot separate them or concentrate them, which are required to enhance the sensitivity of bacteria and virus sensors and to separate blood cells from plasma. In addition to EO fluid flows, a particle force must imparted by the same electric field sustained by the imbedded electrodes. The classical electro-kinetic particle force is DC electrophoresis, the analog of DC EO flow in Equation (1), which is size independent and highly sensitive to surface charge density. Like DC EO, it must be sustained by DC electrodes which cannot sustain a voltage drop exceeding 2 V due to bubble generation and electro-chemical reactions. Hence, on-chip manipulation and concentration are best done with an AC electro-kinetic force. As

in AC EO, this AC particle force would not be sensitive to the surface charge density and particles of different net charge or charge density cannot be separated as in DC electrophoresis of DNA molecules. However, with an abundance of sensors available to offer specificity, separation by surface charge is typically not a function of the micro-fluidic components. Rather, concentrating the particles towards the sensor to reduce the diffusion time is its key task for improving the sensitivity performance. Such concentration is best done with an AC electro-kinetic particle force called dielectrophoresis (DEP).

An applied DC or AC field can induce a dipole on a particle (bacteria) by either double layer charging of the bulk ions or by dielectric polarization of the surface molecules, with opposite polarization at the two poles. For metallic particles, charge transfer from the particle is also a possible mechanism for an anti-symmetric polarization of the double layer. If the field is uniform, the dipole will suffer a torque and will rapidly align with the field. After this rapid alignment, whose transient is negligible in most cases, there is no net force imparted by the uniform far field on the dipole. Dipolar interaction, however, can cause the particles to assemble and align along the field line (Minerick et al., 2003). In the presence of a non-uniform field, a net force results even for an isolated dipole and the resulting motion of the particle is called dielectrophoresis (DEP). DEP drives the bacteria towards either the high field (positive DEP) or weak field (negative DEP) region but is insensitive to the direction of the field. Whether negative or positive DEP occurs, however, is determined by whether the dipole is parallel or anti-parallel to the field. This dipole orientation is on the other hand determined by the specific polarization mechanism behind the dipole formation.

In classical DEP theories (Pohl, 1978), particle polarization is attributed to either molecular polarization captured in the permittivity of the material or by bulk conductivity. A switch between these two mechanisms occurs at the cross-over frequency $\omega=\sigma/\varepsilon$, where σ is the conductivity and ε is the permittivity. At high AC frequencies, the dielectric polarization mechanism with molecular dipoles is at play and conductivity with conduction time scales dominate at frequencies lower than the cross-over. As no net polarization occurs except at an interface, the particle dipole is determined by the conduction of free charges. Multiplying this induced dipole by the a field with a linear gradient to produce a net force and balancing this force by the Stokes drag, the classical DEP theory produces a DEP velocity of the form

$$u_{DEP} = \frac{1}{3\mu}\varepsilon_m R^2 \,\mathrm{Re}[K(\omega)]\nabla\left|E\right|^2 \tag{7}$$

where, for a homogenous spherical particle of radius R, $K(\omega) = (\varepsilon^*_p - \varepsilon^*_m)/(\varepsilon^*_p + 2\,\varepsilon^*_m)$ is the Clausius-Mossotti (CM) factor, and $\varepsilon^* = \varepsilon - i\sigma/\omega$ is the complex permittivity which is dependent on ω, the conductivity σ and the applied field frequency ω. The imaginary part is out of phase with the applied field and, to first order, can be experimentally determined by measuring the torque on a particle in electro-rotation experiments (Hughes and Morgan, 1999). However, the real part of the CM factor is in phase with the applied field and describes the particles polarizability and field induced dipole moment (Arnold et al., 1987). It is clear that the polarization mechanism is due to dielectric polarization at high frequencies but by conduction of free charges in the two media at low frequencies. Depending on the relative magnitudes of the particle and medium conductivity and permittivity, the induced dipoles may or may not align at the two limits. Note also, the double layer capacitor is not described in this classical model. For a latex particle, the particle permittivity and conductivity are both much less than the medium. This classical theory would then predict that $K(\omega)$ is a negative real number for all frequencies, corresponding to negative DEP. This is inconsistent with experimental data on latex particles where a positive DEP is observed at low frequencies (Gagnon and Chang, 2005).

A more complex polarization model (O'Konski, 1960) that includes a conducting Stern layer around the particle surface has been proposed, mostly to reconcile the failure of the classical theory for latex particles. The Stern layer can be shown to modify the effective particle conductivity and permittivity yielding an effective complex particle permittivity in the form

$$\varepsilon_p{}^* = (\varepsilon_p + \varepsilon_{dl}2\lambda/R) - i(4\pi/\omega)(\sigma_p + \sigma_{dl}2\lambda/R) \tag{8}$$

where the Debye screening length λ for the double layer thickness is taken to be the thickness of the Stern layer. The Stern layer conductivity and permittivity are usually also taken to be the same order as the medium permittivity and conductivity or are fitted to data. From the above expressions the charge relaxation time for the particle can be shown to be

$$\tau = \frac{\varepsilon_p + 2\varepsilon_m + \varepsilon_{dl}2\lambda/R}{(2\sigma_m + \sigma_p + \sigma_{dl}2\lambda/R)} \tag{9}$$

This model allows u_{DEP} to change sign from negative DEP to positive DEP below the cross-over frequency (COF), $1/2\pi\tau$ (Pohl, 1978) where the CM factor $K(\omega)$ vanishes. For most bacteria, Re[K] is negative for $\omega >$ COF and the particles move towards the low field region (n-DEP). Positive dielectrophoresis (p-DEP) occurs for $\omega <$ COF. It is interesting to note that both the particle size, R, and the double-layer thickness, $\lambda = (\varepsilon RT/2z^2Fc_o)^{1/2}$, appear in the COF only if a conducting Stern layer is included. In fact, when the double layer is thin at high concentrations and low permittivities, it can be shown that, for latex particles with negligible particle permittivity and conductivity, $\mathrm{COF} \sim 2\pi\sigma_m/\varepsilon_m = 2\pi D/\lambda^2$ for $(\varepsilon_m/\varepsilon_{dl}) >> (\lambda/R)$ and is size-independent. The polarization is dominated by double layer charging from the bulk by the normal (radial) field. Conversely, in the limit of $(\varepsilon_m/\varepsilon_{dl}) << (\lambda/R)$, $\mathrm{COF} \sim 2\pi D/\lambda R$ is particle-size dependent as tangential (angular) conduction through the Stern layer now contributes to the overall conductance. The size independence of COF for strong electrolytes are again inconsistent with experimental data, as seen in Figure 8 where large latex particles and small particles are attracted to regions with different field intensities at the same frequency in a strong electrolyte, indicating that the COF is very much size dependent. An accurate DEP theory is hence still missing. We suspect that the capacitance effect of the double layer, which is not captured in current theories, plays an important role in the COF of DEP velocities.

The classical DEP theory is also inadequate for many pathogens. Double layer, ion channels and surface functional groups have all been shown to change the DEP velocity magnitude and direction. For example, it is known that dead and live bacteria are attracted to regions with low and high fields respectively (Gagnon and Chang, 2005), while such distinction is not reflected in the existing theories.

Despite their failure in capturing the direction of DEP, the current theories do capture the magnitude of the DEP velocity. Comparing Equation (7) to (6), one notices that the potential in the AC EO expression is replaced by the field in the DEP velocity. Consequently, for a unit-order CM factor away from the

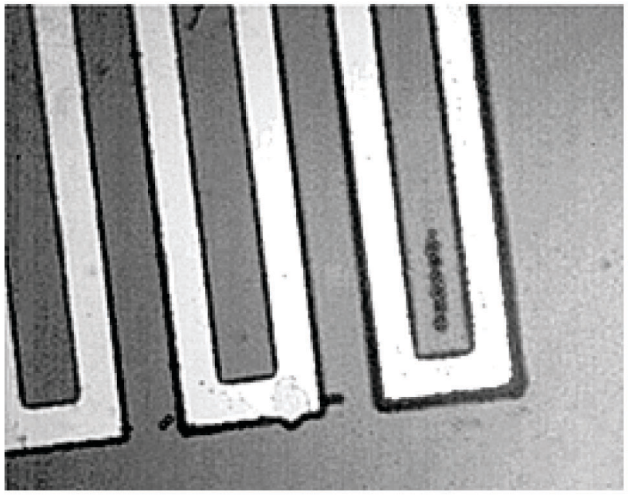

Figure 8. Five micron latex particles are trapped within the gap of wire electrode where the field has a minimum and one-micron particles are trapped at the wire edge where the field is maximum. The former hence exhibits negative DEP while the latter positive DEP.

cross-over frequency, the AC EO convection velocity of Equation (6) and the AC DEP particle velocity of the same device are off by a factor of $(r/L)^2$, where L is the electrode spacing. For micron-sized particles, this corresponds to three to four orders of magnitude and hence DEP velocity rarely exceeds 10 microns/s. Not surprisingly, most DEP studies have indicated that it cannot significantly reduce the diffusion time to the sensor for most realistic device geometries and pathogen concentrations. We believe AC EO convection is the best remedy for the small mobility of DEP. However, DEP is still necessary to achieve the final trapping near the sensor.

AC EO ENHANCED DEP TRAP

AC EO convection has no dependence on particle size and scales much more favourably with the distance from the electrode as discussed earlier. Therefore, EO convection is particularly advantageous for collecting micron/submicron particles from the electrolyte. However, without a particle force and in the absence of particle inertia, the particle trajectory would simply be identical to the streamlines. As much as the flow is incompressible, there are no sinks to the flow field: the stagnation points are either saddle points or centres. Consequently, convection alone cannot concentrate particles and, in fact, in the presence of particle diffusion, only serves to homogenize the particle concentration with high-Peclet dispersion mechanisms (Balakotaiah and Chang, 2003).

It is hence necessary to introduce a particle force like DEP at some location within the flow field. Given the high ratio between AC EO and DEP velocities at $(L/R)^2$, the DEP force cannot overcome the viscous drag force of convection at most locations and would hence be negligible. The only exceptions are at stagnation points and lines where the AC EO flow vanishes. The most optimal stagnation points are those on the surface, either within the electrode gap or on the electrode, as the sensors cannot be suspended at a stagnation point in the bulk. Surface stagnation points are quite common for EO flows as there is a surface slip, as seen in Equations (1) and (6). The surface stagnation points would be where the slip velocity vanishes. Even without surface slip, such as on the substrate within the electrode gap, a stagnation flow with vanishing surface velocities

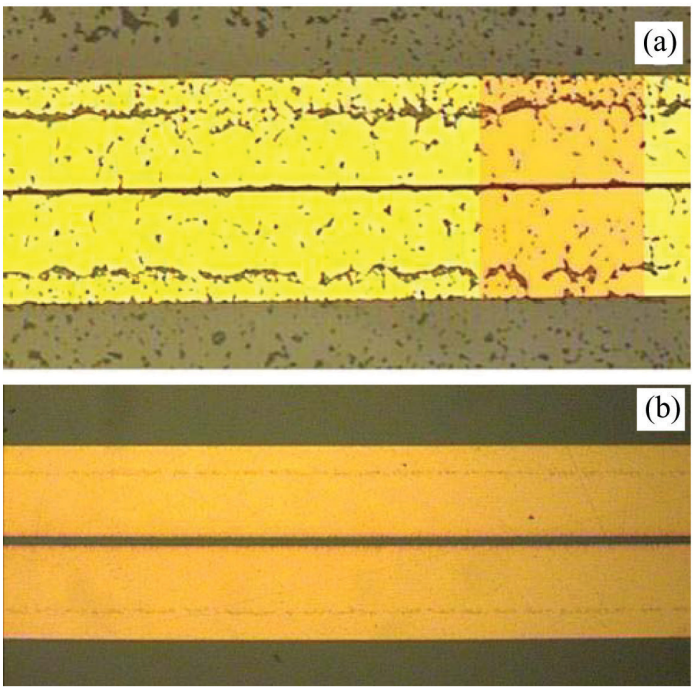

Figure 9. Latex particles and bacteria captured at the $1/\sqrt{2}$ stagnation line of Figures 4 and 5.

can still exist. A simple analysis of the dynamical system near the stagnation flow, describing the trajectory of a particle under both a DEP force and AC EO convection, suggests that the saddle point can be converted into a sink if the stagnation flow is a converging one on the surface and the particle force is towards the surface.

A converging stagnation line is indeed shown in Figure 5 where the stagnation lines on two wide, symmetric parallel electrodes lie at $1/\sqrt{2}$ of the electrode width from the inner edge. Hence, if one employs a positive DEP on the particles in the bulk solution, they should be trapped at these locations. Moreover, the trapping time of all particles would be the channel height divided by large AC EO velocity of Figure 6 and not that divided by the 10 micron/s DEP velocity.

In Figures 9, we show images of latex particles and E Coli being trapped on electrode surfaces using this AC EO-enhanced strategy. The frequency is selected so it is lower than the COF such that a positive DEP force exists at the stagnation line to transform it to a trapping sink. All particles, latex and bacteria, are seen to assemble along the predicted $1/\sqrt{2}$ stagnation line. The particles are trapped within 2 min and the pathogen concentration is as low as one thousand CFU (colony forming units) per cc, roughly the benchmark expected for diagnostic kits.

Trapping within the electrode gap can be achieved by using a frequency higher than COF. The trapped particles can then be released by reducing the frequency below COF, as seen for the wire geometry in Figure 10.

To achieve AC EO enhanced–enhanced trapping, the optimum frequency for AC EO flow, $D/\lambda L$, in Figure 6 must lie on the correct side of COF to ensure trapping on the electrode or within the gap. The easiest design approach is to vary the electrode separation L. Alternatively, if COF has a different permittivity dependence than $D/\lambda L$ such as a –2 power scaling with respect to λ for strong electrolytes, one can also add zwitter ion to tune the permittivity ε and produce maximum AC EO flow on the correct side of COF (Gagnon and Chang, 2005).

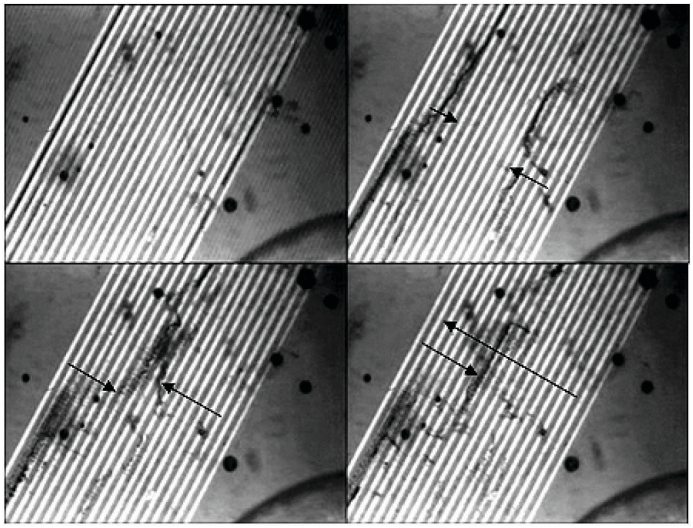

Figure 10. Rapid particle release—Top left: 0 sec.; top right: 0.25 sec.; bottom left: 0.50 sec.; bottom right: 1 sec. Careful look at bottom right image shows the right particle slug overshooting the left particle slug. The applied voltage is 20 V_{RMS} and the applied frequency is 500 kHz.

A biosensor strategically placed at the trapping location would hence enjoy an effective trapped pathogen concentration several orders of magnitude higher than in the bulk, with corresponding increase in sensitive and decrease in response time. There are, however, other particle forces that may oppose the DEP force at the trapping stagnation points or lines. Positive or negative buoyancy force can introduce to a sedimentation velocity, which also scales as R^2, like the DEP velocity of Equation (7). If the sedimentation velocity is not towards the surface, the electric field needs to be increased so that the DEP velocity exceeds the sedimentation velocity. Conversely, a proper sedimentation velocity can replace DEP as the trapping particle force.

At high concentrations, low-permittivity particles can screen the field and hence affect the trapping range of the DEP force. Another particle force that enters at high concentrations is a hydrodynamic particle force that always opposes trapping on the surface: shear-induced migration due to asymmetric particle interaction across a particle when a shear rate gradient exists (Leighton and Acrivos, 1987). The shear induced migration velocity scales as $-\phi R^2 \nabla\gamma$, where ϕ is the particle volume fraction and γ the shear rate U/R for a vortex of dimension R. The shear-induced migration is hence dominant at high concentrations and is always away from the high shear rate region. A dimensionless parameter measuring the relative magnitude between the opposing DEP and shear-induced migration motions of the particle can be obtained from the DEP velocity Equation (7) and the above shear-induced migration velocity, $\chi=(\varepsilon V^2 R^2/\mu L^2 U\phi)$, where L is the electrode separation and V the applied AC rms Voltage. At high concentrations or low χ, shear-induced migration dominates over the trapping DEP mechanism and the pathogens cannot be trapped. In Figure 11, we show suspended ring structures that form above the intended trapping regions at high concentrations when χ is small. Fortunately, for most realistic samples, the pathogen concentration is low and the value of χ is large such that trapping can still be achieved. The only exception is separating blood cells in whole blood with ϕ = .40. Being deformable, blood cells are even more susceptible to shear-induced migration (Zhou and Chang, 2005). Hence, blood cell concentration cannot be achieved at the stagnation lines. In fact, blood cell separation is best done with shear-induced migration alone or pure DEP.

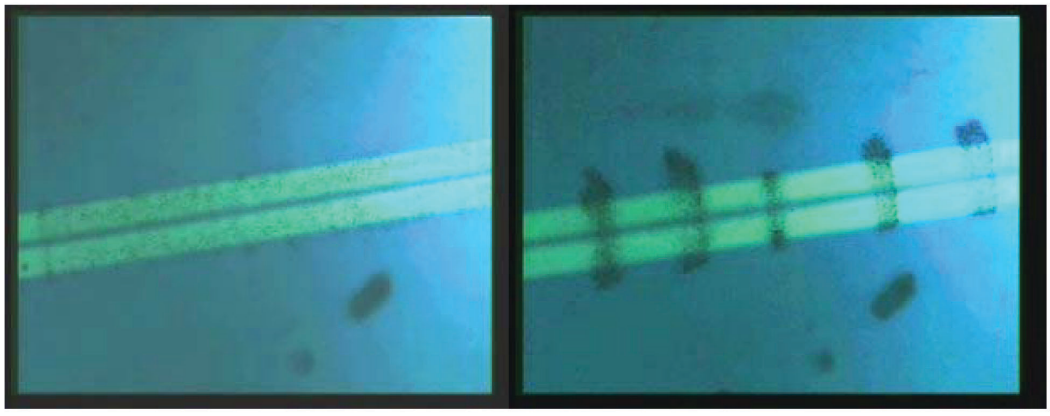

Figure 11. The formation of hollow ring latex particle structures above the same electrodes as Figure 9 when shear-induced migration prevents trapping of the particles. The particles first accumulate within a cylinder, which then undergoes an instability to break up into individual rings.

NANO-PROBES AS PATHOGEN TRAP AND DEP TRANSPORTER

With submicron viruses, the DEP velocity is so small that trapping is also hard to achieve in the presence of any significant flow. An explicit criterion for the cut-off size has not been derived and tested but it is most likely related to a balance between the viscous drag and the DEP force for a particle about a particle radius above the surface or stagnation line. With the boundary effect, the forces do not both have the same R scaling and a distinguished R when the two balance can be derived. One strategy to trap sub-micron pathogens is to increase its dipole moment by docking with a strong induced dipole.

Carbon nanotubes (CNT) and semi-conducting nanowires, representing one of the best examples of novel nanostructures, exhibit a range of extraordinary physical properties, such as extremely small size and high aspect ratio (> 1000), high conductivity or large permittivity—all suggesting that they can produce extremely large dipoles. The dipole fields produced by CNT can be much higher than the applied field in the neighbourhood of the CNT. This enhanced AC field can produce a larger dipole in a nearby pathogen, much like gold colloids are used to enhance AC electro-magnetic fields by ten orders of magnitude in surface-enhance-Raman-scattering (Kneipp et al., 2002). This enhance field can promote dipolar self-assembly and docking of the pathogens with the CNT's along the field lines. Once docked, the CNT-pathogen pair exhibits a high induced dipolar moment and suffers a much larger DEP force that can be trapped by the AC EO enhanced trapping mechanism. The CNT hence serves both as a pathogen trap in the bulk and a pathogen transporter to the trap.

In a recent experiment, we demonstrated this principle with micron-sized bacteria instead of viruses for better monitoring, although fluorescent nano-particles were also successfully tested. A large numbers of single-wall nanotubes (SWNT) is

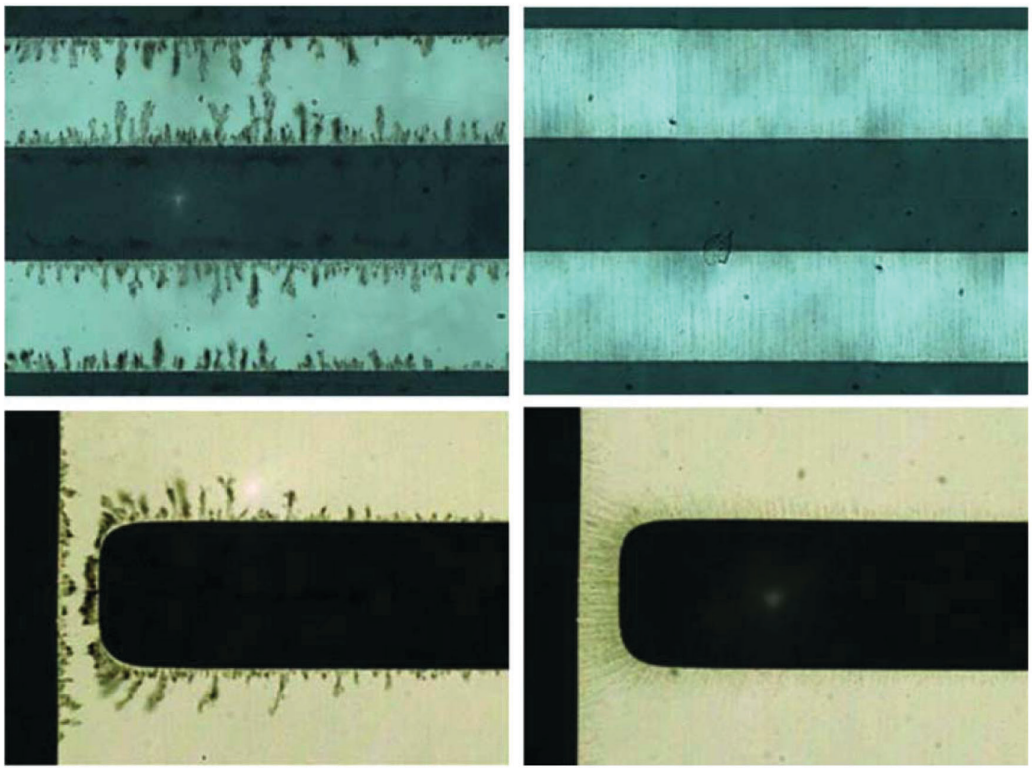

Figure 12. Left two frames: SWNT alignment at 1 KHz for two different electrode configurations. The field and fractal (branched) assemblies are confined to the double layers. Right two frames: the linear alignments at 1 MHz.

dispersed in the sample such that the diffusion length between the bioparticle and the SWNT is determined not by the large average separation between bioparticles ($\sim$1mm) and the electrode sensor but by the much shorter (by a factor of 1000) separation between the bioparticle and SWNT. The latter separation of one micron is essentially the separation between the SWNT and is roughly the same order as the SWNT length. This short separation between SWNT allows the enhanced field to permeate the entire sample.

The electrodes were designed to minimize AC EO flow such that the enhanced negative DEP trapping can be scrutinized directly. Because of the high SWNT concentration, nanotube self-assembly between the electrode gap was detected in a relatively short time, about 0.5–5 min after applying AC electrical field under optical microscopy. The linear aggregates that formed due to induced-dipole-dipole interaction are similar in dimension to SWNT self-assembly in organic solutions or during chemical-vapour deposition with external field. However, the degree of branching of the linear aggregates and whether they bridge the two electrodes are sensitive to the field frequency. As shown in the analysis of the AC EO flow Equation (6) with the effective RC double layer boundary condition, the bulk field diminishes to zero due to double layer screening at frequencies below $D/\lambda L$, which is about 100 kHz for the experiments. On hence expect dipolar self-assembly of linear CNT aggregates across the gap only at frequencies higher than this value. As seen in Figure 12a, the SWNT self-assembly was confined to a thin boundary near the electrode and highly branched at low frequencies ($<$1kHz). Bridging did not occur even after 5 min. When the frequency was increased beyond 1kHz to about 1MHz in Figure 12b, the SWNT self-assembled rapidly from both electrodes to form thin uniform wires that bridged the gap. The wires grew linearly from seeds on each electrode until the other electrode was reached.

Bulk CNT-pathogen docking is demonstrated with 100-nm fluorescent particles replacing pathogens in Figure 13. Unlike bacteria, these particles still exhibit a small positive DEP mobility at the operating frequency of 1 Mhz. Images of the trapped 500-nm or 1 micron fluorescent particle images were recorded at 5 min for three different conditions at frequency 1MHz: fluorescent particles without SWNT, SWNT self-assembly by the AC field was first carried out before the fluorescent particles were added, and when both SWNT and fluorescent particles were mixed before the field was activated. It is clear that the number of collected particles is quite similar for the case without SWNT and the case with pre-templated SWNT. Without SWNT wires, the electrode corners have the highest field and a small number of particles are trapped at that location. With the pre-templated wires bridging the electrodes, the high field region is at the wire and trapping occurs directly onto the wire, although they still tend to favour the ends of the wires closest to the electrode corners. As the particle DEP force is the same for both cases, similar trapping efficiency for the two indicate the corner field without SWNT and the field at the pre-templated wire are comparable in amplitude. In contrast, when SWNT is dispersed in the solution, nearly ten times as many particles are trapped. We attribute this enhanced efficiency to the higher positive DEP mobility of the particles after docking with the SWNT. Docking and enhanced trapping of real bacteria are demonstrated in Figure 14. Trapping of E. coli 10^5 CFU/ml suspended in DI water and SWNT solution were compared. Without SWNT, an extremely small number of bacteria, probably corresponding to a few anomalous ones that exhibit positive DEP at 1 Mhz, were observed at the edge of the electrodes after more than half an hour. With the addition of SWNT, we were able to be observed about ten times as many trapped bacteria, entangled within the SWNT wire between the electrodes and sometimes next to each other, within 5 min.

INTERFACIAL DYNAMICS DUE TO AC POLARIZATION

Many micro-fluidic applications involve drops, sprays and bubbles and it would be desirable to transfer the advantages of electro-kinetic devices for liquids and particles to interfacial flows. Air bubble spacers to isolate different liquid drops in a kit would allow multiple samples to be processed in the same kit. However, simple extension of DC EO flow to displace bubbles proved to be ineffective (Takhistov et al., 2002). DC EO flow of liquid is detected but the flow simply flows through the wetting film around the bubble without displacing it. The longitudinal

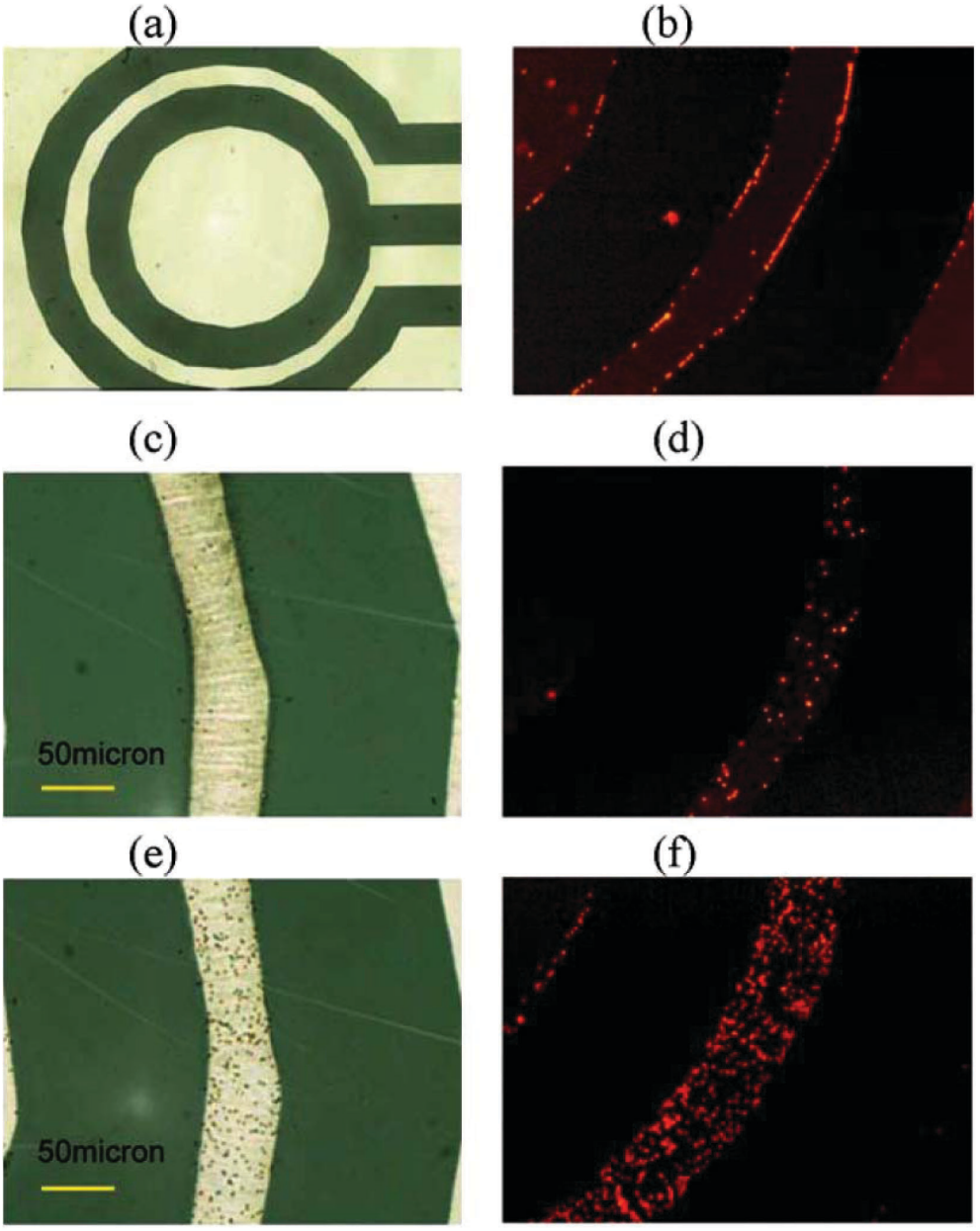

Figure 13. Actual and fluorescent images of fluorescent nano-partilces trapped between two electrodes at 1 MHz. (a) and (b) are without SWNT; (c) and (d) are with pre-assembled SWNT; and (e) and (f) are with a dispersed SWNT and particle suspension.

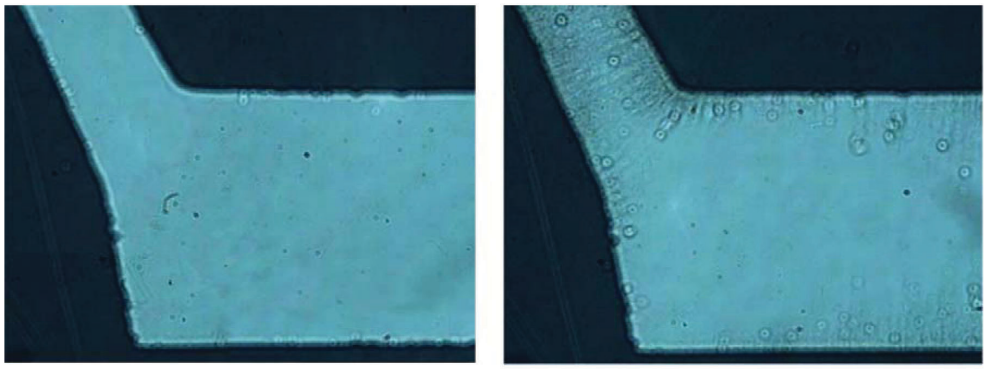

Figure 14. Trapped bacteria with (left frame) and without (right frame) SWNT in the solution. The transparent circles are E Coli bacteria.

field in the wetting film is higher than that upstream of the bubble by a ratio corresponding to the ratio between the capillary and film cross-section area. Since DC EO flow is proportional to the local tangential field, as shown in Equation (1), the velocity in the film is much higher than that upstream but the flow rate, which is the product of the velocity with the cross-section area, remains the same. A perfect liquid flow balance results and the bubble is not displaced. Our solution is to add drop traction with surfactants whose polarity is different from the capillary surface such that the film flow is reduced to almost zero (Takhistov et al., 2002). However, DC EO displacement of bubbles suffers the same disadvantage as DC EO flow, the displacement velocity is extremely low at much less than 1 mm/s.

DC spray mass-spectrometry is a well-developed technology but transferring samples from a diagnostic kit to a mass spectrometer by a DC spray remains an active area of research (Chen et al., 2005b). The obstacle here is to generate enough pressure to overcome the large capillary resistance at the spray orifice. We again use the silica monolith in Figure 1 to provide the necessary pressure. Mass spectrometry remains an excellent diagnostics for chemicals, proteins and even bacteria. Recent development of portable mass spectrometers suggests that interfacing portable diagnostic kits with portable mass spectrometers via electro-sprays will be a promising technology. The chip shown in Figure 1 allows simple transfer from a diagnostic kit to a mass spectrometer. In fact, the same field that is used to pump liquid, pressurize the meniscus and spray can also be used to do capillary electrophoresis or chromatographic separation upstream. The silica monolith itself, with proper functionalization and chemical treatment, can be a good chromatograph substrate (Chen et al., 2005a).

As in single-phase electro-kinetics, AC and DC electro-sprays are found to be quite distinct, with dramatically different aerosol size, charge and flow rates (Yeo et al., 2004, 2005). Field-induced polarization of the double layer seems to be the key mechanism for DC and low-frequency AC sprays, instead of the dielectric polarization mechanism proposed by Taylor and other classical spray theories (Taylor,

1964). In contrast, high-frequency AC sprays with frequency in excess of the inverse RC time are polarized by gas-phase ionization reactions (Lastochkin and Chang, 2005) and hence the liquid drops remain neutral. There are specific advantages to these neutral drops in pathogen detection. As the drops do not undergo Rayleigh fission in flight, individual virus or bacteria could be encapsulated within the drops without being torn apart. As these pathogens are charged, their charge/mass ratio may provide some form of identification. In Yeo et al. (2005), PLA polymers are sprayed out of the AC spray to generate fibres and capsules. The electro-neutrality of the drops also prevents the encapsulated viruses or proteins from being destroyed by the high fields common to DC sprays. Encapsulated viruses may prove to be useful for pathogen detection in the field.

Electro-wetting driven by an AC field allows the handling of multiple samples, encapsulated in individual drops, in a diagnostic kit and it is an active area of research (Cho et al., 2003). However, the classical theories based on Lipmann pressures and DEP-type polarization theory pre-assumes a dielectric polarization. There is evidence that double layer type frequency-dependent field-induced polarization is again at play (Yeo and Chang, 2005). The classical electro-wetting theories also focused only on changes in equilibrium contact angle and interfacial tension, instead of a bulk Maxwell pressure gradient that can produce wetting flow (Yeo and Chang, 2006). Considerable fundamental work is still needed before electro-wetting or spraying dynamics is fully understood.

SUMMARY AND FUTURE WORK

With proper designs, a micro-fluidic platform based on electro-kinetics can offer good mixing, high throughput and larger diagnostic sensitivity, as well as portability, in a totally integrated diagnostic kit isolated from the environment save for electrical contacts. These designs rely on fundamental understandings of the basic physics in AC electro-kinetics and fluid mechanics. The designs also include selection of an optimum AC frequency, as all fluid and particle AC electro-kinetics involve certain RC times due to either double layer charging or dielectric polarization, and proper electrode geometry to achieve mixing or pumping action. A fundamental understanding of particle dynamics, driven by electro-kinetic, gravitational, and hydrodynamic or magnetic forces is crucial when pathogen concentration or debris/blood cell separation must be achieved within the kit.

There is, however, one micro-fluidic operation that has not been scrutinized: particle separation. A design strategy is still missing for electro-kinetic separation components for blood cells, bacteria and size based on their size, deformability, dielectric property, viability (dead-or-alive) and ion-channel activity. For example, septic, sickle and malaria infected blood cells are known to have dramatically different size, shape and ion-channel activity from healthy cells. These are same characteristics that produce different DEP, shear-induced migration and sedimentation mobilities and many of the micro-fluidic technologies can be employed to separate the diseased blood cells for diagnostic purposes. Chip-level cytometry based on some of these forces should be achievable in the near future. However, these forces are for isolated particles and breakdown at high concentration. It is expected that fractionation of concentrated particle suspensions would be difficult and dilution is probably necessary.

Although larger viruses can be trapped with the nano-probes and DEP, smaller molecules like DNAs, proteins and ions cannot be concentrated or separated with these mechanisms on a consistent basis. Docking nano-probes with small bacteria has been shown to enhance the mobility of smaller organisms. The same strategy can be employed for DNAs and proteins. In fact, docking two different nano-probes or micro-particles at the ends of a chromosome may allow DNA stretching and spatially precise genetic probing by a micro-fluidic DEP trap with a gradient in field intensity. Ions and molecule trapping micelles in micellar electro-chromatography can also be trapped and sorted with the particle manipulation techniques. A recent study shows that the intense charge build-up near certain substrate surfaces by field-induced polarization can be used to concentrate charged molecules and ions (Wang et al., 2005). Many non-metallic but conducting granules are indeed nano-porous and ion-specific like the silica monoliths of Figure 1. It is hence not surprising that they can filter and concentrate ions in the presence of a through field. What would be a significant breakthrough would be the use of AC EO or EO flow due to field-induced polarization to enhance the filtration and concentration either at a nano-porous membrane or near an ion-selective granule. It would be the molecular analog of AC EO enhanced trapping for bacteria. Extending the electro-kinetic technologies to molecules and ions would greatly extend the range of the diagnostic targets.

Another important micro-fluidic technology is micro-valving for multi-task and multi-target chips of the future. An enzyme immunoassay kit, for example, requires periodical injection of reagents, mixing and rinsing with buffer solutions. Such operations can only be achieved with valves at intersecting channels. A functioning and cheap on-chip valve is still not available. Such valves will become necessary for the more advanced multi-channel chips.

A multi-sample PCR chip with small on-chip thermal reservoirs could also soon be fabricated using the electro-kinetic platform. AC micro-Ohmic heaters based on electrical resistance heating, a high-resistance version of the loop design in Figure 6, have already been developed. Sensitive thermal sensors, based perhaps on the same nano-probes that enhance electric or electro-magnetic fields, can be integrated with an on-chip feedback control circuit to maintain the temperature of a micro-reservoir despite its small capacitance and the presence of large thermal upsets introduced by multiple PCR samples in transit. A related electro-kinetic technology that is being actively developed to encapsulate multiple PCR solutions is electro-wetting of drops using embedded electrodes (see review by Yeo and Chang, 2005). However, drops come in contact with the electrode and the proteins and DNAs often adhere to the electrodes or are denatured by the high field right at the electrodes. A more attractive encapsulation technique is with immiscible drops within a non-aqueous medium such that the drops are isolated from the electrodes and often screened from the electric field. These drops can be manipulated by the same DEP and AC EO mechanisms as the particles. All these devices can, at least in principle, be based on electro-kinetics driven by on-chip electrodes. Even the removal of DNA from cells via electro-poration is an electro-kinetic phenomenon that can be carried out with the same platform. As mentioned earlier, stretching of the DNA and precise division and amplification of specific DNA segments may be achievable in the near future with colloid-conjugated DNAs.

Despite the various undeveloped and desirable technologies, this reviewer believes that a micro-fluidic platform based on electro-kinetics is now sufficiently mature to merit preliminary integration with the much more advanced biosensor and immuno-assay technologies. Sensors based on enzyme reaction,

fluorescent labelling, optical absorption, Raman scattering etc. can all benefit from the enhanced throughput and sensitivity afforded by the current electro-kinetic devices. Quite fortuitously, antibody conjugation and other functionalization of quantum dots, CNT and other fluorescent and non-fluorescent nano-probes have also recently reached maturity. Instead of using these nano-probes in a human body, their utility in diagnostic kits, in concert with the electro-kinetic technologies that concentrate and sort them, should produce a viable product in the next few years.

ACKNOWLEDGEMENT

Beginning in 2001, I have had the good fortune to work with a talented and diverse group of PhD students and post-docs on electro-kinetic devices and fundamentals, many of them have gone on to micro-fluidic research careers of their own in chemical engineering, electrical engineering, mechanical engineering, bioengineering, food science, mathematics and chemistry departments throughout the world. They are, in chronological order, Alexandra Indeikina, Paul Takhistov of Rutgers, Adrianne Minerick of Miss State, Jayne Wu of Tennessee, Yuxing Ben of Haliburton, Leslie Yeo of Monash (Australia), Dmitry Lastochkin, Zilin Chen, Ronghui Zhou, Ping Wang, Zachary Gagnon, Diana Hou, Siddharth Maheshwari and Shramik Sengupta.

REFERENCES

Ajdari, A., "Pumping Liquids Using Asymmetric Electrode Arrays," Phys. Rev. E **61**, R45–R48 (2000).

Arnold, W. M., H. P. Schwan and U. Zimmermann, "Surface Conductance and Other Properties of Latex Particles Meassured by Electro-rotation," J. Phys. Chem. **91**, 5093-5098 (1987).

Balakotaiah V. and H.-C. Chang, "Hyperbolic Homogenized Models for Thermal and Solutal Dispersion," SIAM J. Applied Math. **63**(4), 1231–1258 (2003).

Barany, S., D. C. Mischuk and J. Prieve, "Superfast Electrophoresis of Conducting Dispersed Particles," J. Colloid Interface Sci. **207**, 240–250 (1998).

Ben, Y. and H.-C. Chang, "Nonlinear Smoluchowski Slip Velocity and Vortex Generation," J. Fluid Mech. **461**, 229-238 (2002).

Ben, Y., E. A. Demekhin and H.-C. Chang, "Superfast Nonlinear Electrokinetics and Electrophoresis," J. Collid Interface Sci. **276**, 483–497 (2004).

Ben, Y. and H.-C. Chang, "CRC MEMS Handbook: Applications," 9–1, 2nd ed., M. Gad-el-Hak, ed., CRC Publishers (2006).

Chen, Z., H.-C. Chang and T. Hobo, "Application of Monolithic Silica for Microfluidic Analysis," Bunseki Kagaku (Jap. Anal. Chem.) **54**(7), 583–592 (2005a).

Chen, Z., P. Wang and H.-C. Chang, "An Electro-Osmotic Micropump Based on Monolithic Silica for Micro-Flow Analyses and Electro-Sprays," Anal. Bioanal. Chem. **382**, 817(2005b).

Cho, S. K., H. Moon and C.-J. Kim, "Creating, Transporting, and Merging Liquid Droplets by Electrowetting Based Actuation for Digital Microfluidic Circuits," J. Microelectromech. Sys. **12**, 70–80 (2003).

DePalma, A., "Cover Story: Microfluidic Analyzers: Slow, Steady Progress," Biosci. Tech. **10** (2005).

Dukhin, S. S., "Electrokinetic Phenomena of the Second Kind and their Applications," Adv. Colloid Interface Sci. **35**, 173–196 (1991).

Gagnon, Z. and H.-C. Chang, "Aligning fast alternating current electroosmotic flow fields and characteristic frequencies with dielectrophoretic traps to achieve rapid bacteria detection," Electrophoresis **26,** 3725–3737(2005).

Gonzalez, A., A. Ramos, N. G. Green, A. Castellanos and H. Morgan, "Fluid Flow Induced by Non-Uniform AC Electrolytes on Micro-Electrodes: A Linear Double Layer Analysis," Phys. Rev. E **61**, 4019–4028 (2000).

Hedberg, C. W. and M. T. Osterholm, "Outbreak of Feed-Borne and Water-Borne Viral Gastroenteritis," Clin. Microbio. Rev. **6**, 199–210 (1993)

Hughes, M. P. and Morgan, H., "Dielectrophoretic Characterization and Separation of Antibody-Coated Submicrometer Latex Spheres," Anal. Chem. **71**, 3441–3445 (1999).

Israelchivili, J. N., "Intermolecular and Surface Forces," Academic Press (1992).

Kneipp, K., H. Kneipp, I. Itzkan, R. R. Dasari and M. S. Feld, "Surface-Enhanced Raman Scattering and Biophysics," J. Phys. Condens. Matter **14**, R597–R624(2002).

Lastochkin, D., R. Zhou, P. Wang, Y. Ben and H.-C. Chang, "Electrokinetic Micropump and Micromixer Design Based on AC Faradaic Polarization," J. Appl. Phys. **96**, 1730–1733 (2004).

Lastochkin, D. and H.-C. Chang, "A High-Frequency Electrospray by Gas Volume Charge," J. Appl. Phys. **97**, 123309–123311 (2005).

Leighton, D. T. and A. Acrivos, "The Shear-Induced Migration of Particles in Concentrated Suspensions," J Fluid Mech. **181**, 415(1987).

Minerick, A., P. Takhistov, R. Zhou and H.-C. Chang, "Manipulation and Characterization of Red Blood Cells with AC Fields in Micro-Devices," Electrophoresis **24**, 3703 – 3717 (2003).

O'Konski, C. T., "Electric Properties of Macromolecules v. Theory of Ionic Polarization in Polyelectrolytes," J. Phys. Chem. **64**, 605–619 (1960).

Pohl, H. A., "Dielectrophoresis," Cambridge University Press, Cambridge (1978).

Probstein, R. B., "PhysicoChemical Hydrodynamics," Wiley (1994).

Ramos, A., A. Gonzalez , A. Castellanos, N. G. Green and H. Morgan, "Pumping of Liquids with AC Voltages Applied to Asymmetric Pairs of Micro-electrodes," Phys. Rev. E **67**, 056302–1–11 (2003).

Squires, T. M. and S. R. Quake, "Microfluidics: Fluid Physics on the Nanoliter Scale," Rev. Mod. Phys. **77**, 977–1026 (2005).

Takhistov, P., A. Indeikina and H.-C. Chang, "Electrokinetic Displacement of Air Bubbles in Microchannels," Phys. Fluids **14**, 1–14 (2002).

Takhistov, P., K. Duginova and H.-C. Chang, "Electrokinetic Mixing Vortices due to Electrolyte Depletion at Microchannel Junctions," J. Colloid and Interfacial Sci. **263**, 133–143 (2003).

Taylor, G. I., "Disintegration of Water Drops in an Electric Field," Proc. R. Soc. Lond. A **280**, 383–397 (1964).

Thamida, S. and H.-C. Chang, "Nonlinear Electrokinetic Ejection and Entrainment Due to Polarization at Nearly Insulated Wedges," Phys. Fluids **14**, 4315–4328 (2002).

Wang S. C., Y. W. Lai, Y. Ben and H.-C. Chang, "Microfluidic Mixing by DC and AC Nonlinear Electrokinetic Vortices," Ind. Eng. Fund Res. **43**, 2902–2911 (2004).
Wang, P., Z. Chen and H.-C. Chang, "A New Electro-Osmotic Pump Housed in Silica Monoliths," Sens. Actuators **113**, 500–509 (2006).
Wang, Y.-C., A. L. Stevens and J. Han, "Million-Fold Preconcentration of Proteins and Peptides by Nanofluidic Filter," Anal. Chem. **77**, 4293–4299 (2005).
Wu, J., Y. Ben, D. Battigelli and H.-C. Chang, "Long-Range AC Electroosmotic Trapping and Detection of Bioparticles," Ind. Eng. Chem. Res. **44**, 2815–2822 (2005).
Yeo, L. Y. and H.-C. Chang, "Static and Spontaneous Electrowetting," Mod. Phys. Lett. B **19**, 549–569 (2005).
Yeo, L. Y. and H.-C. Chang, "Electrowetting Films on Parallel Electrodes," Phys. Rev. E. **73**, 011605–1–16 (2006).
Yeo, L. Y., D. Lastochkin, S.-C. Wang and H.-C. Chang, "A New AC Electrospray Mechanism by Maxwell-Wagner Polarization and Capillary Resonance," Phys. Rev. Lett. **92**, 133902–133904 (2004).
Yeo, L. Y., Z. Gagnon and H.-C. Chang, "AC Electrospray Biomaterials Synthesis," Biomat. **26**, 6122–6128 (2005).
Zeng, S., C.-H. Chen, J. C. Mikkelsen and J. G. Santiago, "Fabrication and Characterization of Electro-osmotic Micro-Pumps," Sens. Actuators B **79**, 107–114 (2001).
Zhou, R. and H.-C. Chang, "Capillary Penetration Failure of Blood Suspensions," J. Colloid Interface Sci. **287**, 647–656 (2005).
Zhou, R., P. Wang and H.-C. Chang, "Bacteria Capture, Concentration and Detection by AC Dielectrophoresis and Self-Assembly of Dispersed Single-Wall Carbon Nanotubes," Electrophoresis (in press).

Manuscript received X X, 2006; revised manuscript received X X, 2006; accepted for publication X X, 2006.